ISSN 1392-1207. MECHANIKA. Vol. 30, No. 4, 2024: 341–346

Multiscale Mixed Elastohydrodynamics in Inclined Fixed Pad Thrust Bearing Involving Surface Roughness

Jinxin ZHU, Yongbin ZHANG
College of Mechanical Engineering, Changzhou University, Changzhou, Jiangsu Province, China,
E-mails: yongbinzhang@cczu.edu.cn (Corresponding author); engmech1@sina.com
https://doi.org/10.5755/j02.mech.35539

1. Introduction

Hydrodynamic thrust bearings are widely used in mechanical engineering for supporting the rotating shafts with the axial load. Their technical requirements are high load-carrying capacities, low friction coefficients and negligible surface wear. They were conventionally designed according to the classical hydrodynamic lubrication theory [1], which is base on the assumptions of the Newtonian fluid, the ideally smooth bearing surface and the isothermal condition. In today's industry, the loads are increasingly heavy and the sliding speeds are more and more high in such bearings. Those assumptions appear difficult to stand and the classical design theory is challenged.

In severe operating conditions, the hydrodynamic film thicknesses in these bearings are much lower than the classical hydrodynamic lubrication theory calculations. For example, in the large-size thrust bearings used in hydropower generators, the hydrodynamic film thicknesses can be reduced to the ultra low values and even vanishing [2-4]. For explaining such phenomena, the effects of the fluid non-Newtonian shear thinning, the surface roughness and the fluid film viscous heating were proposed [5-10]. However, no satisfactory consensus has been reached. It was believed that in the large-size thrust bearing the effect of the surface thermoelastic deformation should be significant and it can directly cause the hydrodynamic film breakdown [2-4]. In micro thrust bearings, the hydrodynamic film thicknesses are also intrinsically very low and often no more than 100 nm [11].

In a hydrodynamic thrust bearing, when the surface separation is low, a lot of new factors such as the effects of the adsorbed layer, the surface roughness and the surface elastic deformation should be involved, as the sizes of these factors are on the same scale with the surface separation. In the classical modeling of the hydrodynamic thrust bearings with surface roughness, whenever the hydrodynamic film thickness is high or low, the effect of the adsorbed layer on the bearing surface was not considered, and the bearing surfaces were even frequently treated as rigid [12-14]. New modeling thus needs to be developed for the hydrodynamic thrust bearing with low clearance by incorporating more realistic factors.

In recent years, deeper recognitions were achieved on the flow in a very small surface separation, which is essentially multiscale and consists of both the adsorbed layer flow and the intermediate continuum fluid flow [15]. For this flow regime, the flow equations have been derived [15]. The research progress in this area makes the present study feasible.

We have studied the effect of the surface elastic deformation in a hydrodynamic micro thrust bearing by considering the effect of the physically adsorbed layer on the bearing surface [16]. As a successive research, the present paper aims to analytically study the combined effects of the adsorbed layer, the surface roughness and the surface elastic deformation in the hydrodynamic inclined fixed pad thrust bearing with low clearance where the multiscale flow occurs. The numerical calculations were made. The film pressure distributions, the surface separation profiles and the carried loads of the bearing have been numerically calculated for different operating conditions. The present study newly reveals the phenomena occurring in this specific bearing obtained from the more realistic mixed lubrication model.

2. Hydrodynamic inclined fixed pad thrust bearing with low clearance involving more realistic factors

Fig. 1 shows the studied hydrodynamic inclined fixed pad thrust bearing with low clearance where the sinusoidal surface roughness with the maximum height R_z is imposed on the stationary surface. In this bearing, the sandwich film occurs in the whole lubricated area and it consists of both the adsorbed layer and the intermediate continuum fluid film [16]. The moving surface with the speed u is assumed as perfectly smooth so that the condition is steady-state. The thickness of the adsorbed layer on either of the bearing surfaces is h_{bf}. Here, the elasticity of

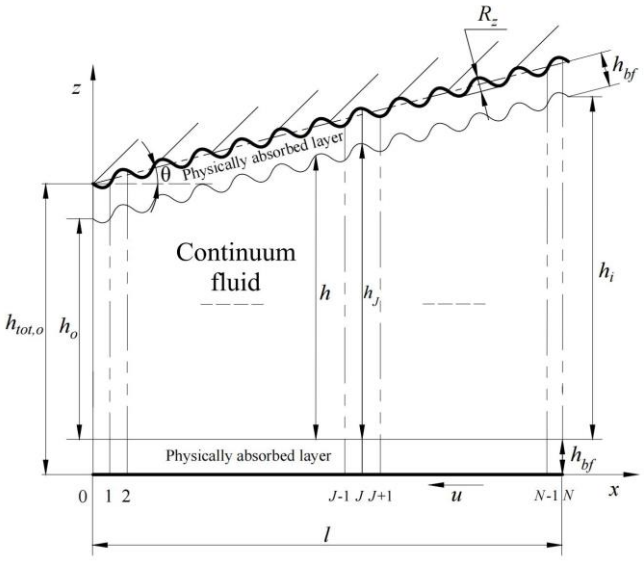

Fig. 1 The studied hydrodynamic inclined fixed pad thrust bearing with low clearance and with the sinusoidal surface roughness imposed on the stationary surface

different surface materials is explored. These materials include steel, non crystalline silica, bronze, silicon and silicon carbonized. The tilting angle and the width of this bearing are respectively θ and l. The thickness of the intermediate continuum fluid film is generally termed as h, and its values on the entrance and exit of the bearing are respectively termed as h_i and h_o. The surface separation on the exit of the bearing is $h_{tot,o}$.

3. Analysis

Here, the used multiscale lubrication analysis is the same with that presented in ref. [16]. For conciseness, this content is not repeated. Considering the surface roughness and the surface elastic deformation, the surface separation on the J^{th} discretized point shown in Fig. 1 is formulated as:

$$h_{tot,J} = h_{oo} + x_J \tan\theta + \frac{R_z}{2}\sin\left(\omega x_J + \varphi\right) - \\ -\frac{2}{\pi E_v}\int_0^l p(s)\ln\left(x_J - s\right)^2 ds, \quad (1)$$

where h_{oo}, ω and φ are respectively constant, R_z is the maximum height of the surface roughness, E_v is the compound Young's modulus of elasticity of two bearing surfaces [16].

For the numerical analysis, the (N+1) discretized points are evenly distributed in the whole hydrodynamic area of the bearing, as shown in Fig. 1.

4. Calculation

Here, the numerical solution procedure is the same with that presented in [16]. The weak, medium and strong fluid-bearing surface interactions have been respectively considered. The parameter values for characterizing these interactions have been shown in [16]. In all the calculations, it was taken that: l = 600 μm, ω = (2.094E–6) rad/m, $\varphi = \pi$. The values of the other operational parameters are the same with those shown in [16]. For different bearing materials, the Young's modulus of elasticity (E) and the Poisson's ratio (μ) are respectively shown in Table 1.

Table 1
Young's modulus of elasticity and Poisson's ratio for different bearing materials

Materials	E, GPa	μ	E_v, GPa
Non crystalline silica	73	0.17	75
Bronze	108	0.32	120
Silicon	190	0.1	192
Steel	193	0.3	209
Silicon carbonized	450	0.25	480

5. Results

5.1. Comparison of the surface separation profiles respectively for elastic steel surfaces and rigid surfaces

Fig. 2, a – c show the comparisons between the surface separation profiles respectively for elastic steel surfaces and rigid surfaces for different fluid-bearing surface interactions when R_z = 4 nm, w = 4000 N/m and u = 4E–4 m/s. Owing to the surface elastic deformation, the original surface roughness is flattened. In the case of the rough surface, for a given load and sliding speed, the fluid-bearing surface interaction appears to have a negligible influence on the shape of the surface separation distribution, but lifts the surface separations in the whole hydrodynamic area if the interaction strength between the fluid and the bearing surface is increased. Whenever the bearing surfaces are rigid or elastically deformed, the surface separations in the whole hydrodynamic area are significantly increased with the increase of the interaction strength between the fluid and the bearing surface. These results are the same with those for the smooth bearing surfaces as shown in [16].

5.2. Comparison of the film pressure profiles respectively for elastic steel surfaces and rigid surfaces

Fig. 3, a – c show the film pressure distributions respectively for elastic steel surfaces and rigid surfaces for different fluid-bearing surface interactions when R_z = 4 nm, w = 4000 N/m and u = 4E–4 m/s. These pressure profiles well correspond to the surface separation distributions in Fig. 2, a – c. For rigid surfaces, we can notice a bit film pressure ripples owing to the surface roughness. But no apparent film pressure ripples are observed for the rough elastic bearing surfaces.

Fig. 4, a – c show the influences of the surface roughness on the film pressure distribution respectively for elastic steel surfaces and rigid surfaces for different fluid-bearing surface interactions when $h_{tot,o}$ = 18 nm and u = 4E–4 m/s. Whenever the bearing surfaces are rigid or elastic, the film pressures are overall increased with the increase of the surface roughness. However, this effect is more significant for rigid surfaces than for elastic surfaces. The effect of the surface roughness on the film pressure appears to be strongly dependent on the fluid-bearing surface interaction whenever the bearing surfaces are rigid or elastically deformed. However, for elastic steel surfaces such a dependence is weaker than for rigid surfaces. We also notice that when the value of R_z is increased to 6 nm, there is a bit film pressure ripples especially for the weak interaction even when the rough bearing surfaces are elastically deformed. However, for the strong fluid-bearing surface interaction the film pressure ripples are largely reduced because of the generated much higher film pressures and the resulting much greater surface elastic deformations as compared to the case of the weak fluid-bearing surface interaction.

5.3. Variations of the carried load of the bearing with the surface roughness respectively for elastic steel surfaces and rigid surfaces

Fig. 5 shows that the carried load of the bearing is significantly increased with the increase of the surface roughness R_z especially for the strong fluid-bearing surface interaction whenever the bearing surfaces are rigid or elastically deformed. However, the increase slope of the bearing load with the surface roughness appears smaller for the elastic steel surfaces than for rigid surfaces. elastically deformed. However, the increase slope of the bearing load with the surface roughness appears smaller for the elastic

steel surfaces than for rigid surfaces. Also, for the same operating condition, the carried load of the bearing for the elastic steel surfaces is significantly smaller than that for rigid surfaces. These phenomena are particularly apparent for the strong fluid-bearing surface interaction. Whenever the bearing surfaces are rigid or elastically deformed, the carried load of the bearing is significantly increased with the increase of the interaction strength between the fluid

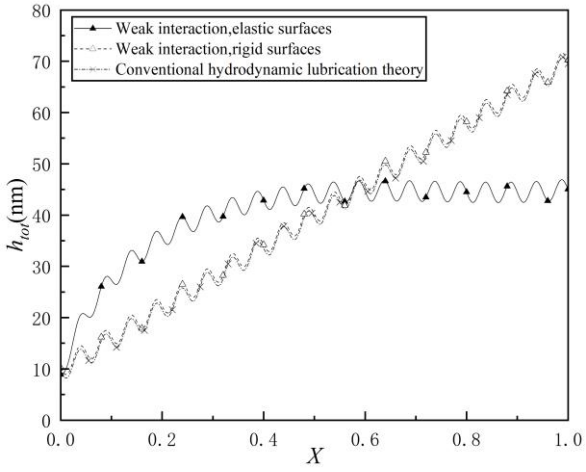

a

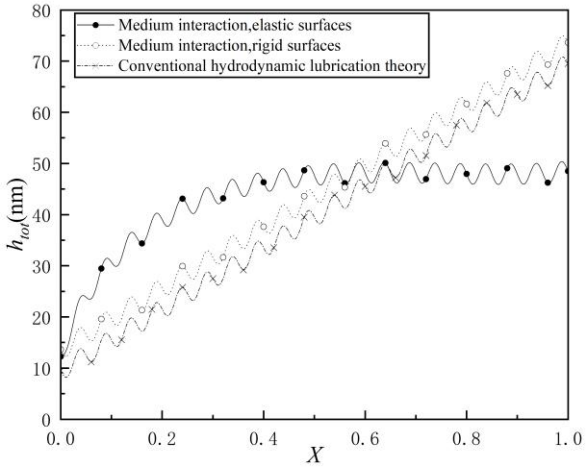

b

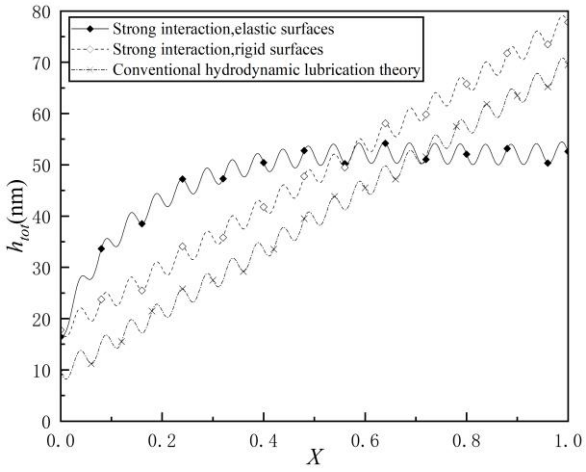

c

Fig. 2 Comparison between the surface separation profiles respectively for elastic steel surfaces and rigid surfaces for different fluid-bearing surface interactions when R_z = 4 nm, w = 4000 N/m and u = 4E–4 m/s: a – for the weak interaction, b – for the medium interaction, c – for the strong interaction

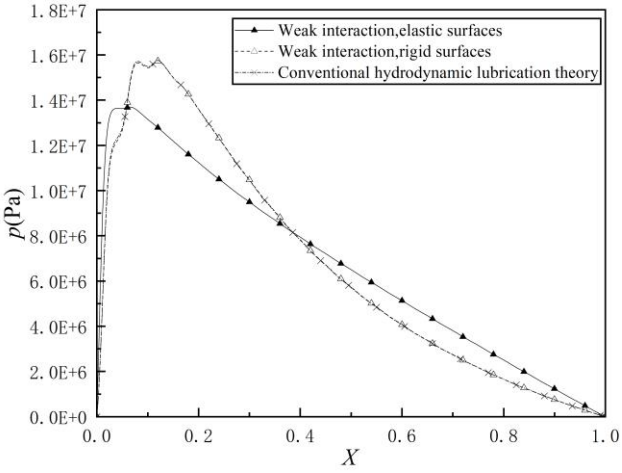

a

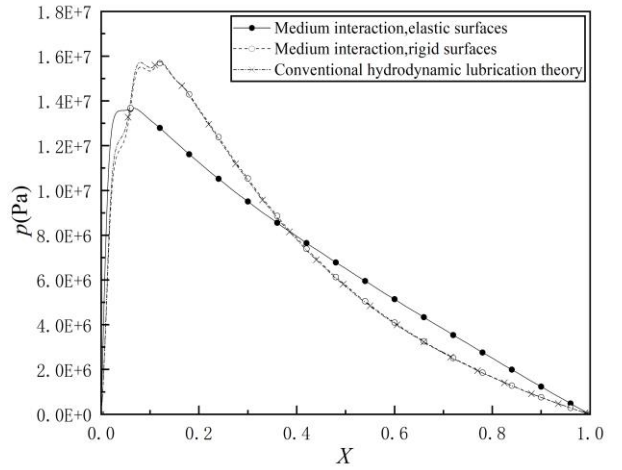

b

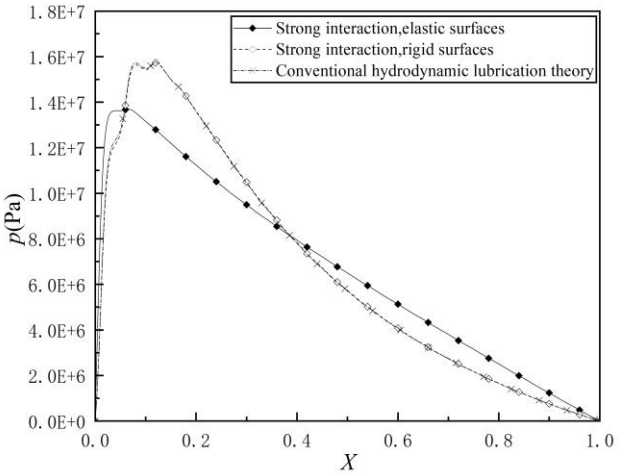

c

Fig. 3 Comparison of the film pressure profiles respectively for elastic steel surfaces and rigid surfaces for different fluid-bearing surface interactions when R_z = 4 nm, w = 4000 N/m and u = 4E–4 m/s: a – for the weak interaction, b – for the medium interaction, c – for the strong interaction

and the bearing surface especially for greater surface roughness. However, this effect is more stronger for rigid surfaces.

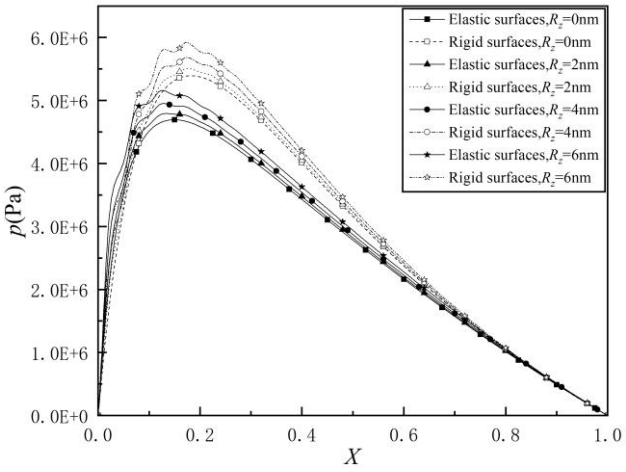

a

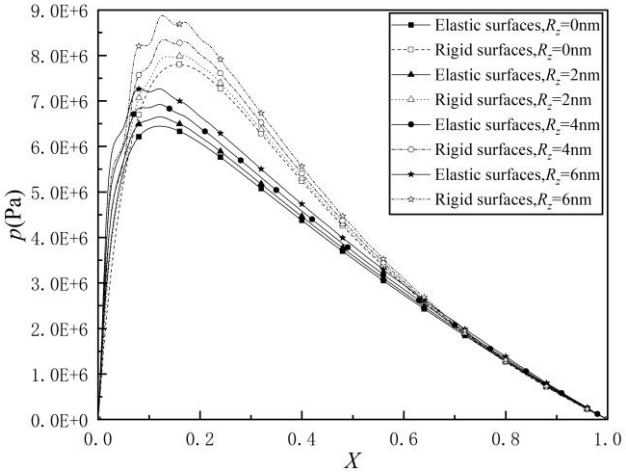

b

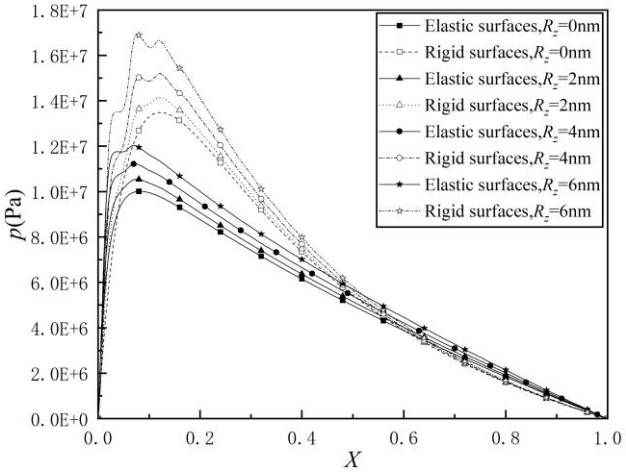

c

Fig. 4 Influences of the surface roughness on the film pressure distribution respectively for elastic steel surfaces and rigid surfaces for different fluid-bearing surface interactions when $h_{tot,o}$ = 18 nm and u = 4E–4 m/s: a – for the weak interaction, b – for the medium interaction, c – for the strong interaction

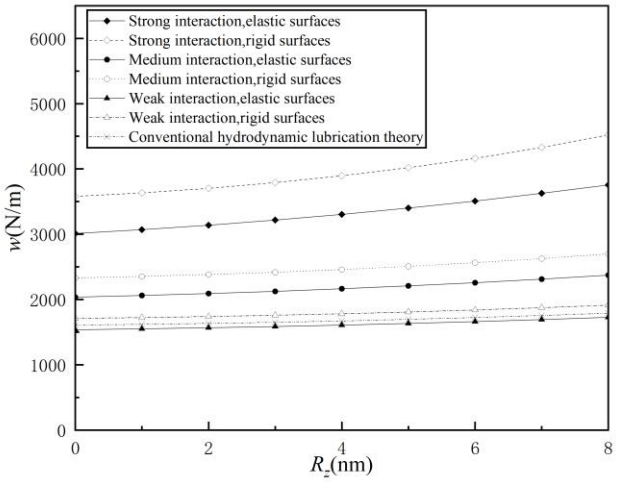

Fig. 5 Variations of the carried load of the bearing with the surface roughness R_z respectively for elastic steel surfaces and rigid surfaces for different fluid-bearing surface interactions when $h_{tot,o}$ = 18 nm and u = 4E–4 m/s

5.4. Performances of the bearing for different surface materials

Fig. 6 shows that when the operation condition is given, the surface separation profile in the bearing is heavily influenced by the bearing surface material. The material with a large Young's modulus of elasticity such as silicon carbonized gives the surface separation profile close to that for rigid surfaces. While the bearing surfaces made of steel gives the surface separation profile significantly deviating from that for rigid surfaces owing to the pronounced surface elastic deformation. The material with a small Young's modulus of elasticity such as non crystalline silica radically modifies the surface separation profile and moves to the outlet zone the location where the maximum surface separation occurs; In this case, the original surface roughness is reduced to the largest as compared to the cases for the other materials.

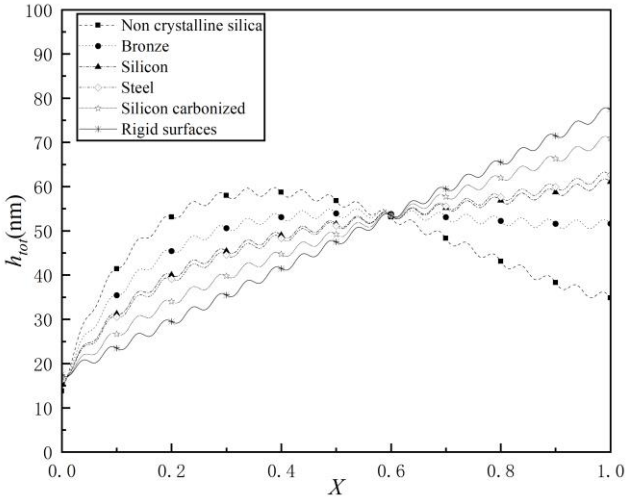

Fig. 6 Comparisons among the surface separation profiles respectively for different bearing surface materials for the medium fluid-bearing surface interaction when R_z = 2 nm, w = 2500 N/m and u = 4E–4 m/s

Fig. 7 shows that when the operating condition is given, the bearing surface materials with different Young's modulus of elasticity give different film pressure distributions owing to the surface elastic deformation. The material of silicon carbonized gives the film pressures very close to those for rigid surfaces. The material of steel gives the film pressure distribution apparently different from that for rigid surfaces. The material of non crystalline silica gives the film pressure distribution the most significantly deviating from that for rigid surfaces. For the material with a small Young's modulus of elasticity, the film pressure ripple is not observed for the given case.

Fig. 8 shows the load (w) versus minimum surface separation ($h_{tot,min}$) curves respectively for different bearing surface materials for the medium fluid-bearing surface interaction when R_z = 2 nm and u = 4E–4 m/s. The slopes of these curves represent the film stiffness for different surface materials. It is shown that when the Young's modulus of elasticity of the surface material is greater, the hydrodynamic film stiffness in the bearing is larger. For a given load, the material with a smaller Young's modulus of elasticity gives a lower value of the minimum surface separation; Or for a given value of the minimum surface separation, the material with a smaller Young's modulus of elasticity gives a smaller bearing load.

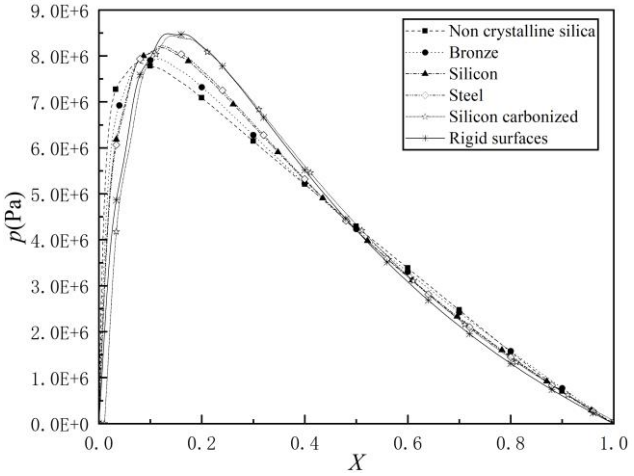

Fig. 7 Comparisons among the film pressure distributions respectively for different bearing surfaces for the medium fluid-bearing surface interaction when R_z = 2 nm, w = 2500 N/m and u = 4E–4 m/s

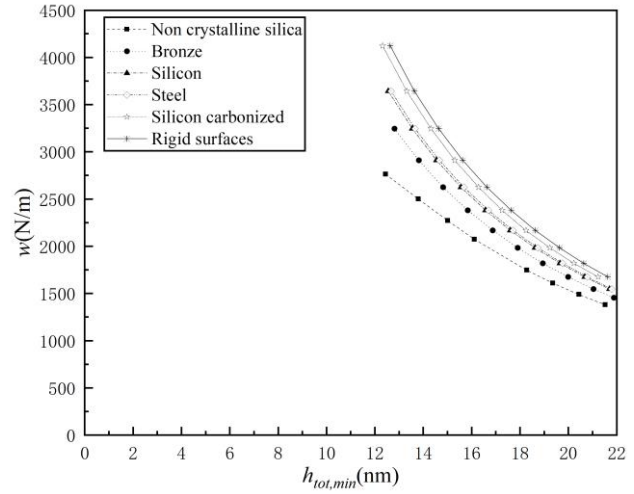

Fig. 8 The load (w) versus minimum surface separation ($h_{tot,min}$) curves respectively for different bearing surface materials for the medium fluid-bearing surface interaction when R_z = 2 nm and u = 4E–4 m/s

6. Conclusions

The combined effects of the adsorbed layer, the surface roughness and the surface elastic deformation are analytically investigated by the multiscale approach in the hydrodynamic inclined fixed pad thrust bearing with low clearance. The coupled bearing surfaces are made of the same material. The moving surface is assumed as perfectly smooth and the stationary surface is imposed with the sinusoidal surface roughness so that the operating condition is steady-state. In the whole hydrodynamic area of this bearing, there is the sandwich film which consists of both the adsorbed layers and the intermediate continuum fluid film. Zhang's closed-form explicit multiscale flow equations were used to respectively describe the flows of the adsorbed layers and the flow of the intermediate continuum fluid. Based on these equations, the numerical calculations were made for the film pressures, the surface separations and the carried loads of the bearing for different surface roughness and different fluid-bearing surface interactions. Based on the calculation results, the conclusions are drawn as follows:

1. Whenever the bearing surfaces are rigid or elastically deformed, the carried load of the bearing is significantly increased with the increase of the surface roughness especially for rigid surfaces and for a strong fluid-bearing surface interaction. However, this increase slope is smaller for elastic surfaces than for rigid surfaces.

2. For the same operating condition, when the Young's modulus of elasticity of the bearing surface material is smaller, the maximum film pressure is lower and the film pressure distribution as well as the surface separation profile in the bearing more significantly deviate from those for rigid surfaces, and the minimum surface separation is smaller.

3. The bearing surface material significantly influences the stiffness of the hydrodynamic film in the bearing. For a given operating condition, smaller the Young's modulus of elasticity of the bearing surface material, smaller the hydrodynamic film stiffness.

4. For the bearing surface material with a large Young's modulus of elasticity such as silicon carbonized, the film pressure and surface separation distributions are close to those for rigid surfaces, and the obvious film pressure ripples can be observed when the maximum height of the surface roughness is only 2nm. However, for the bearing surface with a small Young's modulus of elasticity such as made of non crystalline silica, no film pressure ripples are observed even when the surface roughness is greater, owing to the much greater surface elastic deformation.

5. Due to the surface elastic deformation, the original surface roughness is reduced especially when the film pressures in the bearing are high or the Young's modulus of elasticity of the bearing surface is small.

References

1. **Pinkus, O.; Sternlicht, B.** 1961. Theory of hydrodynamic lubrication, McGraw-Hill, New York.
2. **Ettles, C. M.** 1980. Size effects in tilting pad thrust bearings, Wear 59: 231–245. https://doi.org/10.1016/0043-1648(80)90281-1.
3. **Kawaike, K.; Okano, K.; Furukawa, Y.** 1979. Performance of a large thrust bearing with minimized thermal distortion, ASLE Transactions 22: 125–134. https://doi.org/10.1080/05698197908982908.
4. **Iliev, H.** 1999. Failure analysis of hydro-generator thrust bearing, Wear 225: 913–917. https://doi.org/10.1016/S0043-1648(98)00410-4.
5. **Yadav, S. K.; Sharma, S. C.** 2016. Performance of hydrostatic textured thrust bearing with supply holes operating with non-Newtonian lubricant, Tribology Transactions 59: 408-420. https://doi.org/10.1080/10402004.2015.1083065.
6. **Yadav, S. K.; Sharma, S. C.** 2014. Performance of hydrostatic tilted thrust pad bearings of various recess shapes operating with non-Newtonian lubricant, Finite Elements in Analysis and Design 87: 43-55. https://doi.org/10.1016/j.finel.2014.04.009.
7. **Singh, U. P.** 2020. Mathematical Analysis of Effects of Surface Roughness on Steady Performance of Hydrostatic Thrust Bearings Lubricated with Rabinowitsch Type Fluids, Journal of Applied Fluid Mechanics 13: 1339-1347. https://doi.org/10.36884/JAFM.13.04.30682.
8. **Walicka, A.; Walicka, E.; Jurczak, P.; Falicki, J.** 2014. Thrust bearing with rough surfaces lubricated by an Ellis fluid, International Journal of Applied Mechanics and Engineering 19: 809-822. https://doi.org/10.2478/ijame-2014-0056.
9. **Huebner, K. H.** 1974. A three-dimensional thermohydrodynamic analysis of sector thrust bearings, Tribology Transactions 17: 62-73. https://doi.org/10.1080/05698197408981439.
10. **Heshmat, H.; Pinkus, O.** 1987. Misalignment in thrust bearings including thermal and cavitation effects, Journal of Tribology 109: 108-114. https://doi.org/10.1115/1.3261299.
11. **Papadopoulos, C. I.; Nikolakopoulos, P. G.; Kaiktsis, L.** 2012. Characterization of stiffness and damping in textured sector pad micro thrust bearings using computational fluid dynamics, Journal of Engineering for Gas Turbines and Power 134: 112502. https://doi.org/10.1115/1.4007320.
12. **Walicka, A.; Walicki, E.** 2002. Couple stress and surface roughness effects in curvilinear thrust bearings, International Journal of Applied Mechanics and Engineering 7:109-117.
13. **Sharma, S. C.; Agrawal, N.** 2022. Performance of a spherical hybrid thrust bearing considering the influence of surface irregularities and MR lubricant behavior, Tribology Transactions 65: 457-478. https://doi.org/10.1080/10402004.2022.2050967.
14. **Kumar, V.; Sharma, S. C.** 2018. Influence of dimple geometry and micro-roughness orientation on performance of textured hybrid thrust pad bearing, Meccanica 53: 3579–3606. https://doi.org/10.1007/s11012-018-0897-0.
15. **Zhang, Y. B.** 2020. Modeling of flow in a very small surface separation, Applied Mathematical Modeling 82: 573–586. https://doi.org/10.1016/j.apm.2020.01.069.
16. **Zhu, J. X.; Zhang, Y. B.** 2023. Effect of surface elastic deformation in hydrodynamic inclined fixed pad thrust bearing with low clearance, Mechanika 29: 454-461. https://doi.org/10.5755/j02.mech.33803.

J. Zhu, Y. Zhang

MULTISCALE MIXED ELASTOHYDRODYNAMICS IN INCLINED FIXED PAD THRUST BEARING INVOLVING SURFACE ROUGHNESS AND LOW CLEARANCE

S u m m a r y

The film pressures, surface separation profiles and carried loads of the hydrodynamic inclined fixed pad thrust bearing with the sandwich films were calculated by the multiscale approach when the bearing clearance was low and the combined effects of the adsorbed layer, the surface roughness and the surface elastic deformation were incorporated; The sandwich film consists of two physically adsorbed layers respectively on the coupled bearing surfaces and the intermediate continuum fluid film. The results show that the surface roughness intrinsically generates the film pressure ripples, but the rough surface is somewhat flattened and the film pressure ripples are a bit reduced by the surface elastic deformation. For a given sliding speed and a given original bearing clearance, the surface elastic deformation results in the significant reductions of both the maximum film pressure and the carried load of the bearing especially for a strong fluid-bearing surface interaction. In spite of this, the slope of the increase of the bearing load with the magnitude (R_z) of the surface roughness is nearly the same for the elastic surfaces with that for the rigid surfaces. The presence of the surface roughness does not qualitatively alter the influence of the surface elastic deformation on the performance of the bearing.

Keywords: adsorbed layer, elastic deformation, hydrodynamics, load, pressure, surface roughness, thrust bearing.

Received November 7, 2023
Accepted August 19, 2024